Characteristics of ball-milled PET plastic char for adsorption of different types of aromatic organic pollutants

Hyokchol Mun
Nankai University College of Environmental Science and Engineering
Cholnam Ri
Nankai University College of Environmental Science and Engineering
Qinglong Liu
Nankai University College of Environmental Science and Engineering
Jingchun Tang (tangjch@nankai.edu.cn)
Nankai University https://orcid.org/0000-0001-7633-1701

Research Article

Keywords: Ball-milled plastic char, PET, adsorption, phenanthrene, phenol, 2,4,6-trichlorophenol

Posted Date: February 24th, 2022

DOI: https://doi.org/10.21203/rs.3.rs-1310008/v1

Abstract

Ball-milled plastic char (BMPC) was manufactured by ball-milling of native plastic char (PC) that was synthesized via slow pyrolysis of PET water bottle waste, by which the adsorption characteristics of aqueous phenanthrene, phenol and 2,4,6-trichlorophenol, and its possible mechanisms were investigated. The special surface area of BMPCs increased obviously as the pyrolysis temperature increased, forming large functional groups compared to PCs. Boehm titration showed that total acidic groups of BMPCs decreased significantly with the increase of pyrolysis temperature. The sorption kinetics of three adsorbates was adequately simulated by Pseudo second-order model (R^2 0.99). Langmuir model fitted well the adsorption isotherms of phenanthrene and phenol, while Freundlich model simulated the adsorption isotherm of 2,4,6-trichlorophenol. The adsorption amount of phenanthrene, phenol and 2,4,6-trichlorophenol increased significantly as the pyrolysis temperature increased. The maximum BMPCs adsorption amount reached 21.9mg/g (for phenanthrene), 106mg/g (for phenol) and 303mg/g (for 2,4,6-trichlorophenol) at 25℃ in aqueous solution. FTIR analysis suggested that surface sorption based π-π interaction was dominant mechanism of phenanthrene adsorption, meanwhile, H-bonding between O-containing groups on BMPCs and hydroxyl groups of absorbates was responsible for phenol and 2,4,6-TCP removal. This paper shows that BMPCs can be used as adsorbent for treating aromatic compounds in aqueous environment, and has an economic worth of application.

Introduction

Polyethylene terephthalate (PET), as most important engineering polymer, is harmless to human body, and widely used in all fields of life and industry, such as water bottle, packaging foods, liquid soap and cooking oil, manufacturing films and fibers etc. Enormous consumption of PET plastic leads to abundant accumulation of PET wastes (Ansari et al. 2021), that is, PET waste generation increased from 2015 (13 million tons) to 2019 at a rate of 5.2% annually (Kim et al. 2020). According to official statistics, nearly 20, 000 waste plastic bottles have been thrown away every second, and the recycling rate for these PET bottles is probably 72.1% in Japan, but only 48.3% in Europe and 31% in the United States. Therefore, any new methodologies for the recycling these plastics have been proposed even though its applicability is not so plausible at larger scale (Fuks et al. 2021). Pyrolysis based thermochemical principle is effective technique to convert solid wastes into useable gas, liquid, and solid products in the condition of oxygen-free, and the technology is mature and widely used to treat large amounts of municipal solid wastes (Al-Salem et al. 2017; Dhahak et al. 2020; Muhammad et al. 2015). Recently, it has been proved that the solid by-product (plastic coke) pyrolyzed at temperatures typically between 500℃ and 780℃ (Muhammad et al. 2015) can be efficient for the removal of heavy metals (Fuks et al. 2021; Singh, E. et al. 2020; Singh et al. 2021). It has been improved that the pyrolysis under the inert atmosphere made PET as a highly porous material (Bratek et al. 2013) with pores in the micro-/meso- sizes, which is applicable for different adsorption processes (Parra et al. 2006). Thermal decomposition of PET is initially due to the random disconnection of chains on ester bonds to produce carboxyl and vinyl esters. The thermal decomposition of PET results in the product with high content of aldehides at low temperature treatments, and one with

a high content of aromatics at high temperature treatments (Tang et al. 2015). The specific surface area gives also a significant effect on the adsorption of various organic pollutants (Guo et al. 2017). Ball-milling method, as one of the methods to improve the absorbent properties, is a cost-effective way to increase the specific surface area of carbon materials, therefore, ball-milled biochar has a good adsorption effect on heavy metals, dyes and organic pollutants in water and wastewater (Amusat et al. 2021; Xiang et al. 2020).

The organic pollutants studied in here, such as phenanthrene (PHE), phenol, 2,4,6-trichlorophenol (2,4,6-TCP) are aromatic hydrocarbons, which are all toxic and recalcitrant, and their physiochemical properties are different. PHE is a typical aromatic (3-ring) carbides of polycyclic aromatic hydrocarbons, due to its low solubility to water (1.2mg/L at 25℃) (Zindler et al. 2016), it has high ecotoxicity and long-term persistence, and is considered as an environmental pollutant that can cause acute and chronic diseases to the human health (Kumar et al. 2021). On the other hand, phenol as the basic raw materials of industry, is weak acid and has high toxicity and high solubility to water (85g/L at 25℃) (Guo et al. 2021). It seriously polluted many kinds of industry wastewater, e.g., 6-500 mg/L in refinery wastewater, 28-3, 900 mg/L in coking wastewater, and 2.8-1, 220 mg/L in petrochemical industry wastewater (Mei et al. 2020), and undoubtedly its direct discharge to river will bring serious environmental problems (Yan et al. 2018). 2,4,6-TCP has been reported to cause many health diseases, such as respiration, cardiovascular effects, gastrointestinal effects, and cancer except for nervous toxicity to human (Fan et al. 2011). In addition, the high solubility of 2,4,6-TCP at room temperature (434mg/L in water) (Pei et al. 2013) as well as the stable C-Cl bonds and the positions of chlorine atoms in phenol ring lead to higher toxicity and endurance in the environment comparing with phenol (Tan et al. 2009).

Many methods have been proposed to remove organic pollutants, especially with the development of adsorption method, adsorption has been considered to be the most effective and economic approach to remove different organic pollutants from aqueous environments. For example, adsorption capacities of PHE and phenol were 15.8mg/g(for PHE), 166mg/g (for phenol) with biochar based on Bamboo (Mohammed et al. 2018; Tang et al. 2015) and 367mg/g-2,4,6-TCP with *Loosestrife*-based activated carbon at 25℃, respectively(Fan et al. 2011). PET chemical structure was consisted of the ring structure, so the thermal decomposition of PET-plastic char will also contain many ring-structures, which can effectively adsorb hydrophobic organic materials. In the previous study, the plastic char mainly consisted of mesoporous and macroporous material with adsorption capacities being 3.59–22.2mg/g for methylene blue dye. This indicates that the plastic char can also have good adsorption effect on organic molecules (Bernardo et al. 2012; Sharuddin et al. 2016).

In the study of PET pyrolysis, it is mainly concentrated on the gas and liquid production with the change of thermal decomposition temperature (Dimitrov et al. 2013), however, there were few studies on the characteristics of solid products (Fuks et al. 2021; Parra et al. 2006; Sogancioglu et al. 2017), especially there has been no study on the adsorption and desorption characteristics of organic pollutants by PET plastic char produced from different pyrolysis temperatures. The purpose of this paper is, first, to analyze the physiochemical characteristics of ball-milled plastic chars (BMPCs) produced at different pyrolysis

temperatures through the adsorption capacities of PHE, phenol and 2,4,6-TCP in aqueous environment; second, to investigate the adsorption mechanism of BMPCs and relevant factors.

Materials And Methods

Experimental materials

In this study, Wahaha water bottle was used as raw material for the plastic char. PHE, phenol and 2,4,6-TCP (MERYER 99%) as pollutants, calcium chloride anhydrous ($CaCl_2$) as regulator of ionic strength and sodium azide (NaN_3) as an inhibitor of microbial growth were purchased from Tianjin Huaxun Medical Technology Co., Ltd (China).

The production of BMPCs

Wahaha water bottle was washed and air-dried, and crushed into pieces with the size below 0.5cm×0.5cm. Firstly, 6g PET pieces was pyrolyzed under various pyrolysis temperatures in N_2 gas condition using a tubular furnace (TDRG, Tengda Thermal Technology Co., Ltd., Yixing, China). The pyrolysis experiment was carried out at different temperature (500, 600, 700, and 800℃) for 30 minutes (See detail in Text S1). Secondly, the four kinds of plastic char samples were ball-milled (F-P2000, Focucy, Hunan, China) for 24 hours (See detail in Text S2).

Characterization

A multiple-point Brunauer Emmett Teller(BET) method was applied to measure the surface area, pore size and pore volume of ball-milled plastic char (BMPC) (ASAP2460, Micromeritics, Atlanta, USA), and element analysis was determined using the CHN/O Analyzer (EA3000, Italy). The pH value was measured by a pH meter (PB-10, Sartorius, Goettingen, Germany). SEM analysis (JSM-7800F, JEOL, Japan) were performed to monitor the shapes and surface morphologies of the samples. Raman spectroscopy (SR-500I-A, TEO, USA) was used to characterize the aromatic structure. The functional groups of BMPCs were investigated by Boehm titration method (See detail in Text S3) and Fourier transform infrared spectroscopy (FTIR) measurements (TENSOR 37, BRUKER, Germany). Zeta potential was determined with a Zetasizer Nano ZS90 (Malvern Instruments, Malvern, UK).

Adsorption experiment

Effects of pyrolysis temperature on PHE, phenol and 2,4,6-TCP sorption capacity

PHE, phenol and 2,4,6-TCP were adopted as experimental organic pollutants, respectively. The adsorption characteristics of BMPCs prepared at different pyrolysis temperatures were studied in batches. For PHE adsorption experiment, test solution of PHE at various concentration was prepared with the PHE stock solution diluted with HPLC-grade methanol containing 0.01mol/L $CaCl_2$ (ionic strength adjuster) and 200 mg/L NaN_3 (biocide) solutions. The concentration of methanol in the final solutions was always controlled below 0.1% (v/v) (S. 2001). 2mg of BMPCs were respectively put into 50mL brown vials and then a 40mL aliquot of PHE solution (0.6 mg/L) was poured into the vials. The vials were then tightly capped with Teflon-lined screw caps and vibrated at 150r/min on a reciprocating shaker (HNY-2102C, Honour Instrument Co., Ltd., Tianjin, China) under the condition of the dark at 25℃ for 3 days (Jin et al. 2018; Zhao et al. 2014). As for phenol and 2,4,6-TCP adsorption, samples (10mg) of BMPCs were put into 50mL brown vials and then a 40mL aliquot of phenol and 2,4,6-TCP solution (the initial phenol and 2,4,6-TCP concentration were 10 mg/L and 50 mg/L, respectively) was poured into every vial, and carried out for one day. Other operational condition was same as above. Controls were studied in absence of BMPCs dosage, and controls and samples were repeated least triplicate in every experiment.

Influences of BMPCs dosage on tree absorbates removal efficiency

In order to determine the effective dosage for PHE, phenol and 2,4,6-TCP removal, experiments were carried out according to change of BMPCs dosage (0.025-0.15g/L for 0.6mg/L PHE, 0.125-0.375g/L for 10 mg/L phenol, and 0.125-0.5g/L for 50 mg/L 2,4,6-TCP).

Adsorption kinetics of three absorbates

Initial solution concentration of 0.6mg/L PHE, 10mg/L phenol and 50mg/L 2,4,6-TCP was individually used to describe sorption kinetic of PHE, phenol and 2,4,6-TCP, while BMPCs dosage was 0.05g/L for PHE solution and 0.25g/L for phenol and 2,4,6-TCP solution.

Adsorption isotherm of three absorbates

For the sorption isotherm study, experiments were carried out according to initial concentration change of PHE, phenol and 2,4,6-TCP (0.6-1mg/L for PHE, 10-50mg/L for phenol and 50-100 mg/L for 2,4,6-TCP), in here, dosage in these experiments were 0.05g/L BMPCs per 40mL of PHE solution and 0.25g/L BMPCs per 40mL of phenol and 2,4,6-TCP solution, and experiment was carried out with 72 hr for PHE adsorption and with 24 hr for phenol and 2,4,6-TCP adsorption test.

Analytical methods

The determination of PHE is as follows. 0.5mL of each supernatant that was centrifuged at 4000 r/min for 10min was diluted with 0.5mL of HPLC grade methanol, then followed by filtration using a 0.22 nm

PTEF filter membrane. Agilent HPLC 1260 (USA) equipped with a Thermo Scientific C18 column (25cm×4.6 mm) was used for PHE quantification (Shi et al. 2018). A mixture of acetonitrile and Milipore (80:20) water was eluted at a flow rate of 1 mL/min and system temperature of 30℃, and detected at wavelength of 254nm with a UV detector for PHE determination.

Whilst, the following manipulation as performed for phenol and 2,4,6-TCP. 1.5mL of supernatants that were centrifuged at 4000 r/min for 5min were filtered using a 0.22 nm PTEF filter membrane, and then was measured by HPLC. The method is the same as above, but the wavelength (280nm) and the system temperature (25℃) were different to the above.

Results And Discussion

Physicochemical characterization of BMPCs

The product of PET $(C_{12}H_8O_4)_n$ pyrolysis were gas, waxy and carbonaceous residue (Dhahak et al. 2019), as pyrolysis temperature increases, production yields of solid residues (carbonaceous residue) decreased slightly from 18.9 ± 0.2wt% at 500°C to 13.6 ± 0.2wt% at 800°C. Solid residues from PET pyrolysis were initially lumped like slag, of which, the specific surface area of native plastic chars (PCs) was relatively small, and size of them was arranged from hundreds to thousands of microns (See detail in Table S1). In general, specific surface area is considered to be an important index of the adsorbent sorption ability, therefore, in order to increase specific surface area, produced carbonaceous residues were ball milled for 24 hr. PCs were initially looked like black flakes, couldn`t be distinguished each other, however, after ball-milling, BMPCs could be identified with different pyrolysis temperature. Color of BMPCs was changed from black-brown to strong black as pyrolysis temperature raised (See detail in Figure S1). Specific surface area of BMPCs was increased from 361m²/g to 583m²/g as the pyrolysis temperature raised. pH value is another index to explain adsorbent sorption too (Mohammed et al. 2018; Ri et al. 2022). BMPCs and PCs were weak acid with pH values of 6.41-6.75 and 6.83-6.91, respectively (See detail in Text S1) with the increase of pyrolysis temperature from 500℃ to 800℃. Ball milling made pH values of BMPCs reduced comparing to PCs. The carbon contents of BMPCs increased from 86.4–91.236% when pyrolysis temperature increase from 500℃ to 800℃ (Table 1), whereas hydrogen and oxygen contents were decreased from 4.59–2.48% and from 8.98–6.28%, respectively. According to previous reports, the gas produced during the pyrolysis of plastics such as HDPE, LDPE, PP, PS, PET and PVC contains hydrogen, methane, ethane, ethene, propane, propen, butane and butane (Martı´n-Gullo´n 2001; Sharuddin et al. 2016; Singh, R.K. et al. 2020). In the range of 500-700℃, the content of H_2 gradually increased accompanied by the decrease of CO content with temperature increase, and the contents of CH_4 and CO_2 kept constant. On contrary, the increased of H_2 and CH_4 while the decrease of CO and CO_2 occurred at the stage of 700-800℃. It is worthwhile that the gas fraction of CH_4 increased at higher temperatures during PET pyrolysis (Bai et al. 2020), therefore, BMPC-700 had a high oxygen content more than the others. On the other hand, the ratios of H/C varied from 0.637 to 0.326 concurrently with the aromaticity index (See

detail in Text S4) from 0.805 to 0.965, as the charring temperature raised, from which, evidently implying the evolution of conjugated structure.

Table 1
Physicochemical properties of ball milled plastic char derived from PET water bottle at different temperatures

Sample	BMPC-500	BMPC-600	BMPC-700	BMPC-800
Product yield (%)	18.9	17.3	15.2	13.6
BET Surface Area(m^2/g)	361	439	539	583
Pore Volume(cm^3/g)	0.213	0.258	0.308	0.318
Average Pore size (nm)	2.361	2.347	2.288	2.177
Average Particle Size (μm)	0.934	0.828	0.756	0.524
pH	6.41	6.59	6.61	6.75
C (%)	86.432	89.115	89.225	91.236
H (%)	4.589	4.318	3.6	2.48
O (%)	8.979	6.567	7.175	6.284
O/C [a]	0.0779	0.0553	0.0804	0.0689
H/C [b]	0.637	0.581	0.484	0.326
AI [mol DBE_{AI}/(mol C_{AI})]	0.805	0.834	0.885	0.965
I_D/I_G	0.920	0.934	1.007	1.004
Zeta potential(mv)	-33.8	-34.3	-34.5	-35.2

Note: a; O/C; Atomic mole ratio of oxygen to carbon, b; H/C; Atomic mole ratio of hydrogen to carbon, AI; aromaticity index

The ratio of O/C can reflect the changes in O-containing functional groups of BMPCs with different pyrolysis temperatures (Xiao et al. 2016). The ratios of O/C showed a decreasing trend at 500-600℃ (from 0.0779 to 0.0553) but at 600-700℃ increased again from 0.0553 to 0.0804, and at 800℃ decreased again to 0.0689 (Table 1). BMPCs sorption can be interpreted by the structure-activity relationships between the pyrolysis temperature, H/C atomic ratio and aromatic cluster formation, and sorption capacity. Decreasing the ratio of H/C atomic, the sorption capacity of organic pollutant by char increased linearly with different pyrolysis temperatures. As shown in Table 1, not only specific surface area and surface hydrophobicity of BMPCs but also the aromatization degree was gradually increased with increase in pyrolysis temperature. Zeta potential is an important indicator to characterize the behavior of nanoparticles in colloidal solutions (Biriukov et al. 2020). Zeta potential values of all BMPCs were getting more and more negatively charged as charring temperature raised.

Raman measurement showed that BMPCs like biochar represent two significant peaks at 1350cm^{-1}and 1595cm^{-1}, and the I_D/I_G ratio increased with the increase of pyrolysis temperature (500-800℃), explaining the higher the temperature, the more defects, which may be related to the condensation of small amorphous defects, the removal of some O-containing groups and the succession of aromatic clusters (Guizani et al. 2017). But at 800℃ I_D/I_G ratio was a little bit less than at 700℃ (Fig. 1).

Raman spectroscopy can be used to analyze the structural similarity between the produced materials and the perfect graphite. This analysis is usually used to evaluate the aromatic cluster structure of carbonaceous materials. The D-peak (1350~1400 cm-1) represents the in-plane vibrations of sp3 – bonded carbon atoms that reflects structural defects of graphene structure, while the G-peak (1550~1600cm-1) corresponds to the in-plane stretching vibration of SP2 graphic carbon structures. ID/IG indicates the total number and/or size of graphitic micro domains, and the proportion of the sp3 to sp2 bonding, which can be used to evaluate the degree of disordering/ordering structure (Tang et al. 2015; Xiong et al. 2021). Previous study demonstrated that there exists a well-linear relationship between the intensity ratio of Raman band and atom ratio of O, H to C (Veiga et al. 2021; Xu et al. 2020). The Boehm titration result were summarized in Table S2. For all BMPCs and PCs, surface acidity was dominated by phenolic hydroxyl groups, and lactonic and carboxyl groups on the all BMPCs were hold in less 50% of total acidic functional groups. The total acidic functional group content of BMPCs decreased significantly from 0.0651mol/kg to 0.0501mol/kg, while that of PCs changed between 0.0252mol/kg to 0.0285mol/kg, respectively, as pyrolysis temperature raised. Boehm titration experiment showed that these findings were rather consistent with Raman measurement, ball milling enhanced the surface acidity of adsorbents, and the change of O/C ratio and the pH value of BMPCs were depended on total acidic functional groups (Tang et al. 2015; Xu et al. 2020; Yang et al. 2017). The morphology of all BMPCs was also illuminated by SEM analysis (See detail in Figure S2). All BMPCs particles were mostly less than 2μm of diameter in size, which caused the surface to enlarge and form many pores, and especially, BMPC-800 particles were mostly less than 1μm of diameter in size.

FTIR helped to measure the characteristic stretching frequencies of all BMPCs and elucidate the adsorption mechanism of PHE, phenol and 2,4,6-TCP. FTIR spectra of different BMPCs were compared with previous studies. All BMPCs had peaks of many functional groups, including adsorption band positions at wavelengths of ~3600cm^{-1} (free OH groups representing alcoholic and phenolic), ~3020cm^{-1} (aromatic hydrogen), ~1710cm^{-1}(-COOH), ~1601cm^{-1}(aromatic C= C/C = O), ~1443cm^{-1} (=CH_2 bend; aromatic ring), ~1245cm^{-1} (C-O stretching vibration representing aromatic ethers), and 600~900cm^{-1}(aromatic C-H in plane bending) (Meng et al. 2014; Ri et al. 2022; Singh, R.K. et al. 2020; Tang et al. 2015; Zuo et al. 2021). As shown in Fig. 1, with increasing of thermal decomposition temperature, the richness of functional groups also decreases, especially, the intensity of –OH (3649cm^{-1}), C-H bond (3057cm^{-1}) and =CH_2 bend(-1443 cm^{-1}) were decreased until negligible at 800℃, respectively (Meng et al. 2014). The peak positions of most functional groups shifted from 3637cm^{-1} to 3649cm^{-1} and 1443 cm^{-1} to 1454 cm^{-1} for =CH_2 stretching band, from 3028cm^{-1} to 3057cm^{-1} for C-H

stretching band, from 1708 cm^{-1} to 1716 cm^{-1} for –COOH stretching band, and from 1245cm^{-1} to 1265cm^{-1} for C-O stretching band, whereas negligible for C=C/C=O stretching band. The test of FTIR spectra and Boehm titration explained that BMPCs contained the C atoms bonded to different oxygen-containing groups, such as aromatic C=C/C=O and carboxylic –COOH groups (Amusat et al. 2021; Hu et al. 2014; Parra et al. 2006), and these hydrogen bonds were looser than the tightly bound cyclic OH isomer and OH-ether with increasing of charring temperature. Through the adsorption process of PHE, phenol and 2,4,6-TCP, the characteristics of BMPCs were further explained.

Effects of pyrolysis temperature on PHE, phenol and 2,4,6-TCP sorption capacity

Effects of adsorbents with different pyrolysis temperature on three adsorbates removal efficiency were investigated (Fig. 2). With the increasing pyrolysis temperature, the removal efficiency by using PCs (from 35–68% for PHE, from 28–53% for phenol and from 13–35% for 2,4,6-TCP) and BMPCs (from 72–99% for PHE, from 61–80% for phenol and from 79–90% for 2,4,6-TCP) increased significantly, in particular, 2,4,6-TCP adsorption rate of PCs was more than twice as low as that of BMPCs.

However, 2,4,6-TCP removal efficiency increased from 79–90% at 500-700℃ of pyrolysis temperature, and removal efficiency of BMPC-800 reduced by 82%. The test explained that the removal efficiency of three adsorbates onto BMPCs and PCs was mainly dominated by surface area, and was affected indirectly by O-containing functional groups (Inyang et al. 2014; Lyu, H. et al. 2018). PHE, as a nonionic organic compound, can be hardly ionized, thus its morphological structure may not be so respective to change of the solution pH (Hu et al. 2014), and the adsorption efficiency of phenol is best in the solution pH 6.5 (Lawal et al. 2021), and the TCP removal decreases significantly with initial pH of the solution changed from pH 2 to 12 (Pei et al. 2013; Tan et al. 2009).

The effect of adsorbent dosage on PHE, phenol and 2,4,6-TCP removal

Effects of BMPCs dosage on PHE, phenol and 2,4,6-TCP removal efficiency were shown as Fig. 3. PHE removal efficiency enhanced about from 53–99%, when four kinds of BMPCs dosage was increased from 0.025g/L to 0.15g/L at 0.6 mg/L PHE, phenol removal efficiency enhanced about from 35–99% with increasing BMPCs dosage from 0.05g/L to 0.375g/L at 10 mg/L phenol, and 2,4,6-TCP removal efficiency increased from about 40–99% with BMPCs dosage from 0.125g/L to 0.5g/L at 50mg/L 2,4,6-TCP. PHE and phenol removal efficiency of BMPCs significantly increased with pyrolysis temperature under equal dosage condition, especially, the removal effect of BMPC-800 was better than BMPC-500 and BMPC-600, whilst the adsorption effect was almost no difference compared with BMPC-700, there was rather a slight tendency to shrink. In case of 2,4,6-TCP removal efficiency, BMPC-600 and BMPC-700 had a good removal rate, however, the removal rate of BMPC-800 decreased with the increase of pyrolysis temperature. From the test, in order to demonstrate the characteristics of each BMPCs, the optimal dosage of BMPCs used in subsequent trials was determined to be 0.05g/L for PHE adsorption study and 0.25g/L for phenol and 2,4,6-TCP adsorption study.

Sorption kinetic of PHE, phenol and 2,4,6-TCP on BMPCs

The adsorption kinetics of PHE, phenol and 2,4,6-TCP on BMPCs, were considered via pseudo-first order kinetic model and pseudo-second order model in this work (SM 1) (Mohammed et al. 2018; Wang et al. 2020; Zaghouane-Boudiaf and Boutahala 2011). Sorption kinetic of different pollutants on BMPCs was shown in Fig. 4. Most of PHE, phenol and 2,4,6-TCP were rapidly adsorbed to BMPCs in less than one hour (over 95%), and the apparent adsorption equilibrium was achieved within 72 hours for PHE adsorption (8.6, 9.5, 11.5 and 11.7mg/g), 24 hours for phenol adsorption (25, 27.5, 30 and 31mg/g) and 24 hours for 2,4,6-TCP adsorption (153.8, 178.6, 181.8 and 156.3mg/g). Adsorption capacity of BMPCs increased significantly with increasing pyrolysis temperature in the both (PHE and phenol) cases (Fig. 4A and 4D), whereas adsorption capacity of BMPC-800 was not significantly different comparing to BMPC-700. In addition, 2,4,6-TCP adsorption capacity of BMPC-800 decreased significantly comparing to others (Fig. 4G). Pseudo-first order kinetic model (Fig. 4B, E and H) is the well-known and reliable model for the initial rapid response, and as for the pseudo-second order model (Fig. 4C, F and I), it is assumed that the adsorption rate relies on the number of active sites on the adsorbent surface as a rate constraint step (Hu et al. 2014; Tang et al. 2015).

As expected, pseudo second-order kinetic model fits the best for three kinds of organic pollutants sorption study. In sorption kinetics, R^2 of BMPCs for the pseudo first order model (0.799-0.821 for PHE, 0.72-0.8 for phenol, and 0.73-0.77 for 2,4,6-TCP) were smaller than that of pseudo-second order model (R^2>0.99), which showed that pseudo-second order models described the kinetic adsorption process well. Table S3 shows that the adsorption kinetic parameters, in which the adsorption process of PHE, phenol and 2,4,6-TCP on BMPCs accords with pseudo-second-order kinetics, and reasonably the adsorption rate relates to the number of active sites on the adsorbent surface and the sorption of these pollutants predominantly occurred by chemisorption mechanism (Inyang et al. 2014).

Isotherm models of PHE, phenol and 2,4,6-TCP sorption

By establishing the adsorption isotherm model, the adsorption capacity and equilibrium constant of PHE, phenol and 2,4,6-TCP on BMPCs were derived, and Langmuir and Freundlich model equations were applied to describe the adsorption isotherm in detail (SM 2) (Fan et al. 2011; Godlewska et al. 2019; Hu et al. 2014; Lv and Li 2020; Mohammed et al. 2018).

Figure 5 was shown adsorption isotherm of PHE, phenol and 2,4,6-TCP on BMPCs, and for three absorbates, the sorption data was fitted using Langmuir and Freundlich models (See detail in Table S4). The result showed that two models illustrated the sorption isotherm data of three absorbates well (R^2 > 0.92), wherein, for PHE sorption isotherm, the correlation coefficients R^2 of two models decreased from 0.969 to 0.951 (Langmuir model) and from 0.951 to 0.921 (Freundlich model), and, for phenol sorption isotherm, R^2 values of Langmuir model decreased from 0.998 to 0.994 and R^2 values of Freundlich model increased from 0.991 to 0.995, meanwhile, for 2,4,6-TCP sorption isotherm, R^2 values of two models

increased from 0.993 to 0.998 (Langmuir model) and from 0.996 to 0.998 (Freundlich model) with the pyrolysis temperature increase. Adsorption isotherm data explained that for PHE and phenol adsorption on BMPCs Langmuir model gave better fit than Freundlich model, however, for 2,4,6-TCP adsorption on BMPCs Freundlich model fit better than Langmuir model, and Langmuir model fit well in 2,4,6-TCP adsorption on BMPC-800. K_L, Langmuir constant as a measure index of affinity between adsorbent and adsorbate, increased significantly with pyrolysis temperature increase for PHE and phenol sorption isotherm, suggesting that the adsorption capacities increased from 16.69mg/g to 21.91mg/g (for PHE) and from 90.9mg/g to 106.4mg/g (for phenol), however, for 2,4,6-TCP adsorption K_L values were non-linear with pyrolysis temperature, resulting that the adsorption capacities increased from 263mg/g to 303mg/g (500-700℃ of pyrolysis temperature), and at 800℃ adsorption capacity was 270mg/g. K_F and $1/n$, the Freundlich constants corresponding to adsorption capacity and adsorption intensity, represented that adsorption was favorable, in here, all the $1/n$ values were below 1 and decreased non-linearly, and K_F values changed linearly with pyrolysis temperature. Based on the hypothesis of Langmuir isotherm, adsorption occurs at a specific-uniform surface position within the adsorbents, and is considered as single-layer adsorption, meanwhile, Freundlich isotherm is an empirical equation, describing the adsorption on heterogeneous surfaces (Lawal et al. 2021; Wang et al. 2020). In previous studies, surface adsorption seems likely the dominant mechanism at low concentrations (especially, below 1% of its solubility) (Kong et al. 2011). The adsorption capacities for phenol and 2,4,6-TCP are function of molecular weight and cross-sectional area, and are in direct proportion to the hydrophobicity of adsorbate. In addition, with the increase of chlorination degree, the adsorption capacity also increases. Due to chlorine group as an electron-withdrawing group, the increase of chlorine base makes the electron density in the aromatic ring lower (Denizli et al. 2004; Hamdaoui and Naffrechoux 2007), so leading to enhanced adsorption.

Sorption mechanism of PHE, phenol and 2,4,6-TCP onto BMPCs

In order to clarify the adsorption mechanism of three adsorbates on BMPCs, FTIR spectra before and after sorption was performed. As shown in Fig. 6, the peaks position and intensity of FTIR after adsorption shift significantly.

For the adsorption of three adsorbates on BMPC-500 (Fig. 6(a)), the peak corresponding to vibration of free –OH bond (3649 cm^{-1}) was disappeared after adsorption, such shifts were represented in every FTIR study of BMPCs adsorption. The band at 3028 cm^{-1} (aromatic H_2) was shifted to 3024 cm^{-1} for PHE and phenol adsorption, and the intensity of the peak was increased significantly. After adsorption, the peaks corresponding to –COOH and aromatic C = C/C = O were shifted from 1708 cm^{-1} and 1601 cm^{-1} to 1712 cm^{-1} and 1597 cm^{-1} after phenol and PHE adsorption, respectively, and the intensity of two peaks was increased after adsorption of tree adsorbates. The peaks at 1443 cm^{-1} and 1245 cm^{-1} assigned to $=CH_2$ bend (aromatic ring) and C-O stretching band was shifted to 1467cm^{-1} (for 2,4,6-TCP), 1469 cm^{-1} (for phenol), 1226 cm^{-1} (for phenol and 2,4,6-TCP), and 1243 cm^{-1} (for PHE), respectively, in here, not only the

position of the peaks were shifted, but also was increased significantly in the intensity of the vibration (Pei et al. 2013; Wo et al. 2018; Zhao et al. 2018). This study suggested that three adsorbates attended on the adsorption of BMPC-500 through π-π interaction and O-containing functional groups played in sorption. With the pyrolysis temperature increase, even though the positions of the BMPCs functional groups shifted in a little range, FTIR study of BMPCs was similar to that of BMPC-500 after adsorption of three adsorbates (Fig. 6(b), (c) and (d)). Furthermore, the peaks intensity between 1000 cm^{-1} and 1800 cm^{-1} corresponding aromatic ring got stronger after 2,4,6-TCP and phenol adsorption than after PHE adsorption. This test explained that specific surface area was the main factor of adsorbents adsorption in this study, and π-π interaction and functional groups such as carboxylic –COOH, aromatic C=O/C=C and so on enhanced the characteristics of adsorbents, possibly due to O-containing groups' exposure after ball-milling (Lyu, H.H. et al. 2018), and hydroxyl groups of phenol and 2,4,6-TCP could interact with O-containing groups on BMPCs through H-bonding (Pei et al. 2013).

Conclusions

Native plastic char from PET water bottles (PCs) with pyrolysis temperature between 500℃ and 800℃ could adsorb aromatic compounds such as PHE, phenol and 2,4,6-TCP, and special surface area of PCs increased significantly with raising pyrolysis temperature, however, the adsorption efficiency was not good. The ball-milling method increased the area of PCs by more than two times, and also enhanced the adsorption ability of PHE, phenol and 2,4,6 -TCP in aqueous solutions due to exposure functional groups of adsorbents surface. Specific surfaces of BMPCs and adsorption amount of PHE, phenol and 2,4,6-TCP on BMPCs also increased as pyrolysis temperature raised. Recently, the amount of plastic waste in the world has been explosively increasing, and how treating plastic waste controllably, efficiently as well as future-oriented is the great challenge facing to human community. The method proposed in this paper has certain guiding significance for the pyrolysis treatment of PET plastic wastes and its application, and for the adsorption removal effect of organic pollutants in water environment.

Declarations

Supplementary Information

The online version contains supplementary material available at xxx

Author contribution

All authors contributed to the study conception and design. Conceptualization, methodology, formal analysis, investigation, and writing-original draft were performed by Hyokchol Mun. Jingchun Tang participated in writing–review & editing, Resources, Supervision and Project administration. Formal analysis and editing were performed by Cholnam Ri, and Resources and editing were performed by Qinglong Liu. All authors read and approved the final manuscript.

Funding

This research was financially supported by the National Natural Science Foundation of China (41807363, U1806216), the National Key R&D Program of China (2018YFC182002), and the 111program, Ministry of Education, China (T2017002).

Data availability

Not applicable

Ethics approval and consent to participate Not applicable.

Consent for publication Not applicable.

Competing interests The authors declare no competing interests.

References

1. Al-Salem SM, Antelava A, Constantinou A, Manos G, Dutta A (2017) A review on thermal and catalytic pyrolysis of plastic solid waste (PSW). J Environ Manage 197:177–198. https://doi.org/10.1016/j.jenvman.2017.03.084
2. Amusat SO, Kebede TG, Dube S, Nindi MM (2021) Ball-milling synthesis of biochar and biochar–based nanocomposites and prospects for removal of emerging contaminants: A review. J Water Process Eng 41. https://doi.org/10.1016/j.jwpe.2021.101993
3. Ansari KB, Hassan SZ, Bhoi R, Ahmad E (2021) Co-pyrolysis of biomass and plastic wastes: A review on reactants synergy, catalyst impact, process parameter, hydrocarbon fuel potential, COVID-19. J Environ Chem Eng 9(6). https://doi.org/ARTN 106436
4. Bai B, Liu Y, Zhang H, Zhou F, Han X, Wang Q, Jin H (2020) Experimental investigation on gasification characteristics of polyethylene terephthalate (PET) microplastics in supercritical water. Fuel 262. https://doi.org/10.1016/j.fuel.2019.116630
5. Bernardo M, Lapa N, Goncalves M, Mendes B, Pinto F, Fonseca I, Lopes H (2012) Physico-chemical properties of chars obtained in the co-pyrolysis of waste mixtures. J Hazard Mater 219:196–202. https://doi.org/10.1016/j.jhazmat.2012.03.077
6. Biriukov D, Fibich P, Předota M (2020) Zeta Potential Determination from Molecular Simulations. J Phys Chem C 124(5):3159–3170. https://doi.org/10.1021/acs.jpcc.9b11371
7. Bratek W, Swiatkowski A, Pakula M, Biniak S, Bystrzejewski M, Szmigielski R (2013) Characteristics of activated carbon prepared from waste PET by carbon dioxide activation. J Anal Appl Pyrol 100:192–198. https://doi.org/10.1016/j.jaap.2012.12.021
8. Denizli A, Cihangir N, Rad AY, Taner M, Alsancak G (2004) Removal of chlorophenols from synthetic solutions using Phanerochaete chrysosporium. Process Biochem 39(12):2025–2030.

https://doi.org/10.1016/j.procbio.2003.10.003

9. Dhahak A, Grimmer C, Neumann A, Ruger C, Sklorz M, Streibel T, Zimmermann R, Mauviel G, Burkle-Vitzthum V (2020) Real time monitoring of slow pyrolysis of polyethylene terephthalate (PET) by different mass spectrometric techniques. Waste Manag 106:226–239. https://doi.org/10.1016/j.wasman.2020.03.028
10. Dhahak A, Hild G, Rouaud M, Mauviel G, Burkle-Vitzthum V (2019) Slow pyrolysis of polyethylene terephthalate: Online monitoring of gas production and quantitative analysis of waxy products. J Anal Appl Pyrol 142. https://doi.org/10.1016/j.jaap.2019.104664
11. Dimitrov N, Krehula K, Ptiček Siročić L, Hrnjak-Murgić A, Z (2013) Analysis of recycled PET bottles products by pyrolysis-gas chromatography. Polym Degrad Stab 98(5):972–979. https://doi.org/10.1016/j.polymdegradstab.2013.02.013
12. Fan JL, Zhang J, Zhang CL, Ren LA, Shi QQ (2011) Adsorption of 2,4,6-trichlorophenol from aqueous solution onto activated carbon derived from loosestrife. Desalination 267(2–3):139–146. https://doi.org/10.1016/j.desal.2010.09.016
13. Fuks L, Herdzik-Koniecko I, Rogowski M (2021) Carbon obtained from waste polyethylene terephthalate (PET) containers as potential sorbent of radionuclides from the contaminated aqueous solutions. Int J Environ Sci Technol 18(11):3527–3538. https://doi.org/10.1007/s13762-020-03102-3
14. Godlewska P, Siatecka A, Konczak M, Oleszczuk P (2019) Adsorption capacity of phenanthrene and pyrene to engineered carbon-based adsorbents produced from sewage sludge or sewage sludge-biomass mixture in various gaseous conditions. Bioresource Technol 280:421–429. https://doi.org/10.1016/j.biortech.2019.02.021
15. Guizani C, Haddad K, Limousy L, Jeguirim M (2017) New insights on the structural evolution of biomass char upon pyrolysis as revealed by the Raman spectroscopy and elemental analysis. Carbon 119:519–521. https://doi.org/10.1016/j.carbon.2017.04.078
16. Guo H, Li HF, Jing CAY, Wang XB (2021) Soluble polymers with intrinsic porosity for efficient removal of phenolic compounds from water. Micropor Mesopor Mat 319. https://doi.org/ARTN 111068
17. Guo W, Ai Y, Men B, Wang S (2017) Adsorption of phenanthrene and pyrene by biochar produced from the excess sludge: experimental studies and theoretical analysis. Int J Environ Sci Technol 14(9):1889–1896. https://doi.org/10.1007/s13762-017-1272-8
18. Hamdaoui O, Naffrechoux E (2007) Modeling of adsorption isotherms of phenol and chlorophenols onto granular activated carbon. Part I. Two-parameter models and equations allowing determination of thermodynamic parameters. J Hazard Mater 147(1–2):381–394. https://doi.org/10.1016/j.jhazmat.2007.01.021
19. Hu Y, He YY, Wang XW, Wei CH (2014) Efficient adsorption of phenanthrene by simply synthesized hydrophobic MCM-41 molecular sieves. Appl Surf Sci 311:825–830. https://doi.org/10.1016/j.apsusc.2014.05.173

20. Inyang M, Gao B, Zimmerman A, Zhang M, Chen H (2014) Synthesis, characterization, and dye sorption ability of carbon nanotube–biochar nanocomposites. Chem Eng J 236:39–46. https://doi.org/10.1016/j.cej.2013.09.074
21. Jin J, Sun K, Yang Y, Wang Z, Han L, Wang X, Wu F, Xing B (2018) Comparison between Soil- and Biochar-Derived Humic Acids: Composition, Conformation, and Phenanthrene Sorption. Environ Sci Technol 52(4):1880–1888. https://doi.org/10.1021/acs.est.7b04999
22. Kim S, Park C, Lee J (2020) Reduction of polycyclic compounds and biphenyls generated by pyrolysis of industrial plastic waste by using supported metal catalysts: A case study of polyethylene terephthalate treatment. J Hazard Mater 392:122464. https://doi.org/10.1016/j.jhazmat.2020.122464
23. Kong H, He J, Gao Y, Wu H, Zhu X (2011) Cosorption of phenanthrene and mercury(II) from aqueous solution by soybean stalk-based biochar. J Agric Food Chem 59(22):12116–12123. https://doi.org/10.1021/jf202924a
24. Kumar JA, Krithiga T, Anand KV, Sathish S, Namasivayam SKR, Renita AA, Hosseini-Bandegharaei A, Praveenkumar TR, Rajasimman M, Bhat NS, Dutta S (2021) Kinetics and regression analysis of phenanthrene adsorption on the nanocomposite of CaO and activated carbon: Characterization, regeneration, and mechanistic approach. J Mol Liq 334. https://doi.org/ARTN 116080
25. Lawal AA, Hassan MA, Farid MAA, Yasim-Anuar TAT, Samsudin MH, Yusoff MZM, Zakaria MR, Mokhtar MN, Shirai Y (2021) Adsorption mechanism and effectiveness of phenol and tannic acid removal by biochar produced from oil palm frond using steam pyrolysis. Environ Pollut 269. https://doi.org/ARTN 116197
26. Lv XF, Li SF (2020) Graphene Oxide-Crospolyvinylpyrrolidone Hybrid Microspheres for the Efficient Adsorption of 2,4,6-Trichlorophenol. Acs Omega 5(30):18862–18871. https://doi.org/10.1021/acsomega.0c02028
27. Lyu H, Gao B, He F, Zimmerman AR, Ding C, Huang H, Tang J (2018) Effects of ball milling on the physicochemical and sorptive properties of biochar: Experimental observations and governing mechanisms. Environ Pollut 233:54–63. https://doi.org/10.1016/j.envpol.2017.10.037
28. Lyu HH, Gao B, He F, Zimmerman AR, Ding C, Tang JC, Crittenden JC (2018) Experimental and modeling investigations of ball-milled biochar for the removal of aqueous methylene blue. Chem Eng J 335:110–119. https://doi.org/10.1016/j.cej.2017.10.130
29. Martı´n-Gullo´n (2001) Kinetic model for the pyrolysis and combustion of poly-(ethylene terephthalate) (PET). J Anal Appl Pyrol 58–59:635–650
30. Mei X, Li JH, Jing CC, Fang CH, Liu Y, Wang Y, Liu J, Bi SQ, Chen Y, Xiao YY, Yang X, Xiao YF, Wu S, Ding Y (2020) Separation and recovery of phenols from an aqueous solution by a green membrane system. Journal of Cleaner Production 251. https://doi.org/ARTN 119675
31. Meng FR, Yu JL, Tahmasebi A, Han YN, Zhao H, Lucas J, Wall T (2014) Characteristics of Chars from Low-Temperature Pyrolysis of Lignite. Energ Fuel 28(1):275–284. https://doi.org/10.1021/ef401423s

32. Mohammed NAS, Abu-Zurayk RA, Hamadneh I, Al-Dujaili AH (2018) Phenol adsorption on biochar prepared from the pine fruit shells: Equilibrium, kinetic and thermodynamics studies. J Environ Manage 226:377–385. https://doi.org/10.1016/j.jenvman.2018.08.033
33. Muhammad C, Onwudili JA, Williams PT (2015) Thermal Degradation of Real-World Waste Plastics and Simulated Mixed Plastics in a Two-Stage Pyrolysis–Catalysis Reactor for Fuel Production. Energy Fuels 29(4):2601–2609. https://doi.org/10.1021/ef502749h
34. Parra JB, Ania CO, Arenillas A, Rubiera F, Pis JJ, Palacios JM (2006) Structural changes in polyethylene terephthalate (PET) waste materials caused by pyrolysis and CO2 activation. Adsorpt Sci Technol 24(5):439–449. https://doi.org/Doi 10.1260/026361706779849735
35. Pei ZG, Li LY, Sun LX, Zhang SZ, Shan XQ, Yang S, Wen B (2013) Adsorption characteristics of 1,2,4-trichlorobenzene, 2,4,6-trichlorophenol, 2-naphthol and naphthalene on graphene and graphene oxide. Carbon 51:156–163. https://doi.org/10.1016/j.carbon.2012.08.024
36. Ri C, Tang J, Liu F, Lyu H, Li F (2022) Enhanced microbial reduction of aqueous hexavalent chromium by Shewanella oneidensis MR-1 with biochar as electron shuttle. J Environ Sci (China) 113:12–25. https://doi.org/10.1016/j.jes.2021.05.023
37. S., L. Sorption of Phenanthrene by Reference Smectites.Environ. Sci. Technol.35:3456–3461
38. Sharuddin SDA, Abnisa F, Daud WMAW, Aroua MK (2016) A review on pyrolysis of plastic wastes. Energ Convers Manage 115:308–326. https://doi.org/10.1016/j.enconman.2016.02.037
39. Shi Z, Zhang F, Wang C (2018) Adsorption of phenanthrene by earthworms - A pathway for understanding the fate of hydrophobic organic contaminants in soil-earthworm systems. J Environ Manage 212:115–120. https://doi.org/10.1016/j.jenvman.2018.01.079
40. Singh E, Kumar A, Khapre A, Saikia P, Shukla SK, Kumar S (2020) Efficient removal of arsenic using plastic waste char: Prevailing mechanism and sorption performance. J Water Process Eng 33. https://doi.org/10.1016/j.jwpe.2019.101095
41. Singh E, Kumar A, Mishra R, You SM, Singh L, Kumar S, Kumar R (2021) Pyrolysis of waste biomass and plastics for production of biochar and its use for removal of heavy metals from aqueous solution. Bioresource Technol 320. https://doi.org/ARTN 124278
42. Singh RK, Ruj B, Sadhukhan AK, Gupta P (2020) A TG-FTIR investigation on the co-pyrolysis of the waste HDPE, PP, PS and PET under high heating conditions. J Energy Inst 93(3):1020–1035. https://doi.org/10.1016/j.joei.2019.09.003
43. Sogancioglu M, Yucel A, Yel E, Ahmetli G (2017) Production of Epoxy Composite from the Pyrolysis Char of Washed PET Wastes. Enrgy Proced 118:216–220. https://doi.org/10.1016/j.egypro.2017.07.022
44. Tan IA, Ahmad AL, Hameed BH (2009) Adsorption isotherms, kinetics, thermodynamics and desorption studies of 2,4,6-trichlorophenol on oil palm empty fruit bunch-based activated carbon. J Hazard Mater 164(2–3):473–482. https://doi.org/10.1016/j.jhazmat.2008.08.025
45. Tang J, Lv H, Gong Y, Huang Y (2015) Preparation and characterization of a novel graphene/biochar composite for aqueous phenanthrene and mercury removal. Bioresour Technol 196:355–363.

https://doi.org/10.1016/j.biortech.2015.07.047

46. Veiga PAD, Cerqueira MH, Goncalves MG, Matos TTD, Pantano G, Schultz J, de Andrade JB, Mangrich AS (2021) Upgrading from batch to continuous flow process for the pyrolysis of sugarcane bagasse: Structural characterization of the biochars produced. J Environ Manage 285. https://doi.org/ARTN 112145
47. Wang XQ, Guo ZZ, Hu Z, Ngo HH, Liang S, Zhang J (2020) Adsorption of phenanthrene from aqueous solutions by biochar derived from an ammoniation-hydrothermal method. Sci Total Environ 733. https://doi.org/ARTN 139267
48. Wo J, Ge DD, Huang ZY, He Y (2018) Morphological Characteristics of Chars Obtained from Low-Temperature Pyrolysis of Pulverized Lignite. J Energ Eng 144(3). https://doi.org/Artn 04018016
49. Xiang W, Zhang XY, Chen KQ, Fang JN, He F, Hu X, Tsang DCW, Ok YS, Gao B (2020) Enhanced adsorption performance and governing mechanisms of ball-milled biochar for the removal of volatile organic compounds (VOCs). Chemical Engineering Journal 385. https://doi.org/ARTN 123842
50. Xiao X, Chen Z, Chen B (2016) H/C atomic ratio as a smart linkage between pyrolytic temperatures, aromatic clusters and sorption properties of biochars derived from diverse precursory materials. Sci Rep 6:22644. https://doi.org/10.1038/srep22644
51. Xiong J, Xu JL, Zhou MG, Zhao W, Chen C, Wang MX, Tan WF, Koopal L (2021) Quantitative Characterization of the Site Density and the Charged State of Functional Groups on Biochar. ACS Sustain Chem Eng 9(6):2600–2608. https://doi.org/10.1021/acssuschemeng.0c09051
52. Xu J, Liu J, Ling P, Zhang X, Xu K, He L, Wang Y, Su S, Hu S, Xiang J (2020) Raman spectroscopy of biochar from the pyrolysis of three typical Chinese biomasses: A novel method for rapidly evaluating the biochar property. Energy 202. https://doi.org/10.1016/j.energy.2020.117644
53. Yan WW, Sun FQ, Liu JB, Zhou Y (2018) Enhanced anaerobic phenol degradation by conductive materials via EPS and microbial community alteration. Chem Eng J 352:1–9. https://doi.org/10.1016/j.cej.2018.06.187
54. Yang C-H, Nguyen QD, Chen T-H, Helal AS, Li J, Chang J-K (2017) Functional Group-Dependent Supercapacitive and Aging Properties of Activated Carbon Electrodes in Organic Electrolyte. ACS Sustain Chem Eng 6(1):1208–1214. https://doi.org/10.1021/acssuschemeng.7b03492
55. Zaghouane-Boudiaf H, Boutahala M (2011) Kinetic analysis of 2,4,5-trichlorophenol adsorption onto acid-activated montmorillonite from aqueous solution. Int J Miner Process 100(3–4):72–78. https://doi.org/10.1016/j.minpro.2011.04.011
56. Zhao B, O'Connor D, Zhang JL, Peng TY, Shen ZT, Tsang DCW, Hou DY (2018) Effect of pyrolysis temperature, heating rate, and residence time on rapeseed stem derived biochar. J Clean Prod 174:977–987. https://doi.org/10.1016/j.jclepro.2017.11.013
57. Zhao J, Wang Z, Zhao Q, Xing B (2014) Adsorption of phenanthrene on multilayer graphene as affected by surfactant and exfoliation. Environ Sci Technol 48(1):331–339. https://doi.org/10.1021/es403873r

58. Zindler F, Glomstad B, Altin D, Liu JF, Jenssen BM, Booth AM (2016) Phenanthrene Bioavailability and Toxicity to Daphnia magna in the Presence of Carbon Nanotubes with Different Physicochemical Properties. Environ Sci Technol 50(22):12446–12454
59. Zuo ZL, Luo SY, Liu SH, Zhang JK, Yu QB, Bi XJ (2021) Thermokinetics of mass-loss behavior on direct reduction of copper slag by waste plastic char. Chem Eng J 405. https://doi.org/ARTN 126671

Figures

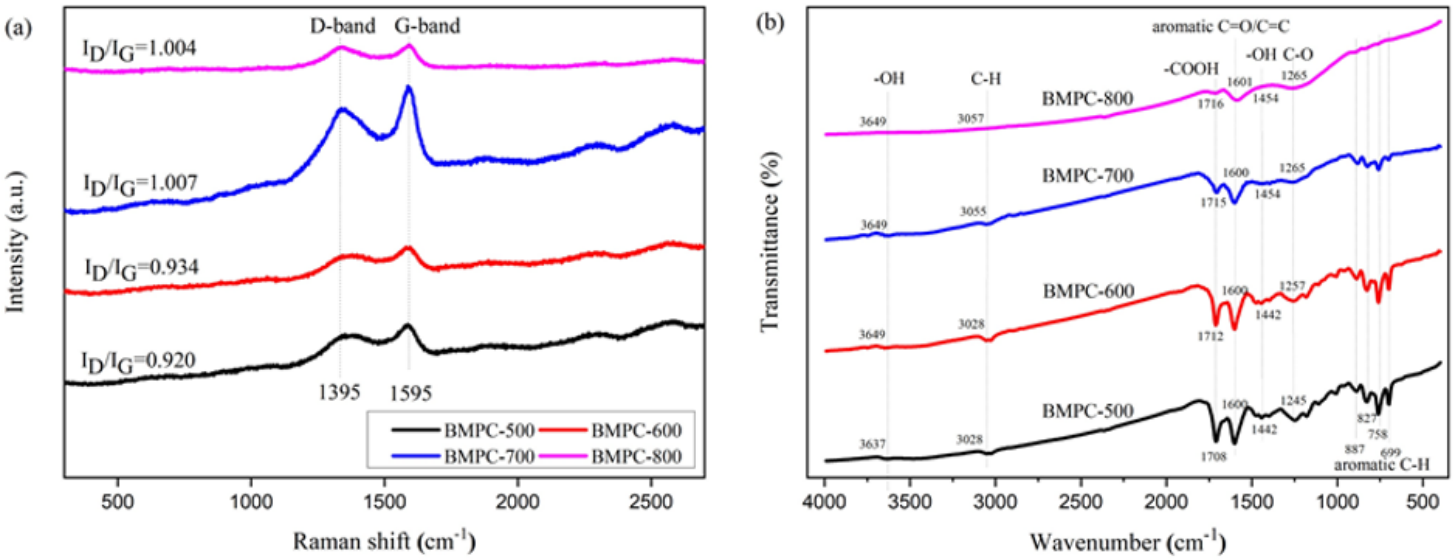

Figure 1

Raman (a) and FTIR (b) spectra of BMPCs derived from PET soft bottle at different pyrolysis temperature

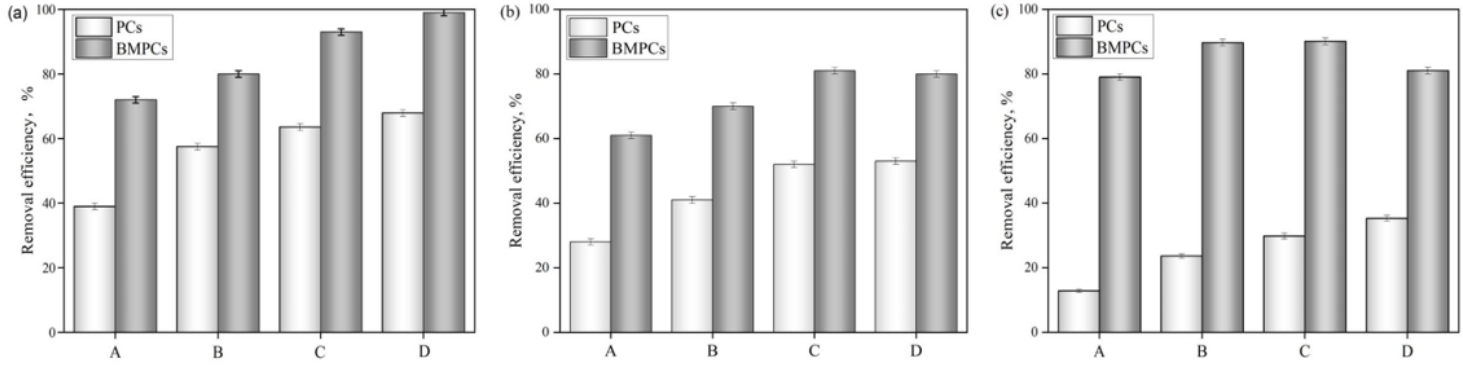

Figure 2

Comparing with the removal efficiency of PHE, phenol and 2,4,6-TCP by using PCs and BMPCs.

(a): PHE removal efficiency at 0.6mg/L of PHE; solution volume 40mL, the adsorbent dosage of PCs and BMPCs was 0.05g/L respectively, pH 6.4-6.9, equilibrium time is three days, temperature 25°C. (b): phenol

removal efficiency at 10mg/L of phenol; solution volume 40mL, the adsorbent dosage of PCs and BMPCs was0.25g/L respectively, pH 6.4-6.9, equilibrium time is one day, temperature 25℃. (c): 2,4,6-TCP removal efficiency at 50mg/L of 2,4,6- TCP; solution volume 40mL, pH 6.4-6.9, the adsorbent dosage of PCs and BMPCs was 0.25g/L respectively, equilibrium time is one day, room temperature (25℃). A; PC-500 and BMPC-500, B; PC-600 and BMPC-600, C; PC-700 and BMPC-700, D; PC-800 and BMPC-800.

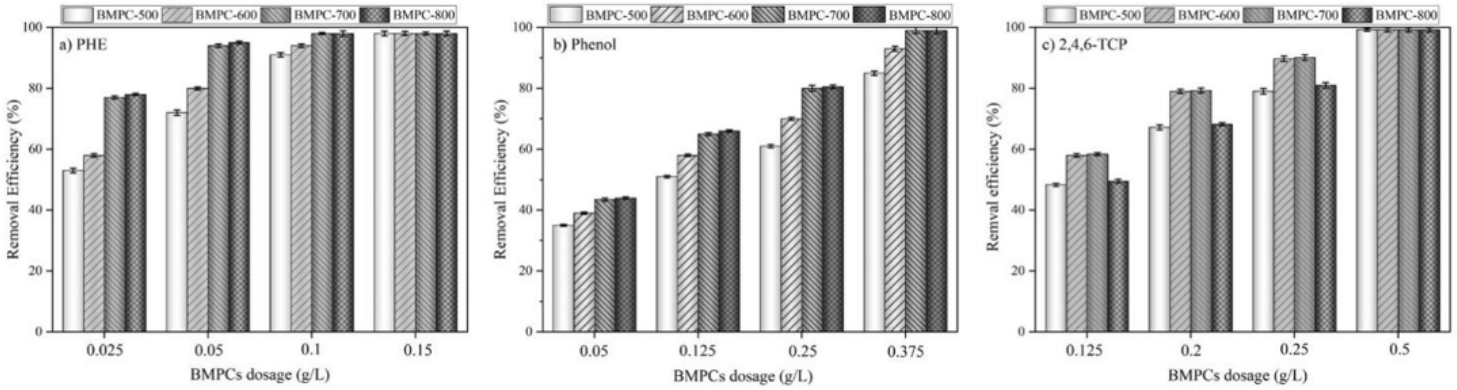

Figure 3

Effects of adsorbents dosage on PHE, phenol and 2,4,6-TCP removal efficiency: a) PHE removal efficiency at 0.6 mg/L of PHE; solution volume was 40mL, pH 6.4-6.8, equilibrium time is three days, temperature 25℃. b) phenol removal efficiency at 10 mg/L of phenol; solution volume was 40mL, pH 6.4-6.8, equilibrium time is one day, temperature 25℃. c) 2,4,6-TCP removal efficiency at 50 mg/L of 2,4,6-TCP; solution volume was 40mL, pH 6.4-6.8, equilibrium time is one day, temperature 25℃.

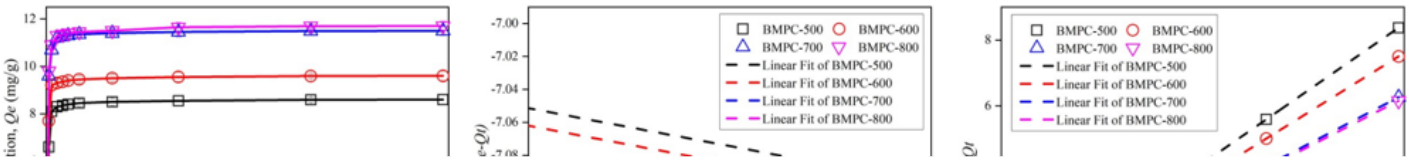

Figure 4

Sorption of kinetics of PHE (A-C), phenol(D-F) and 2,4,6-TCP(G-I). Experimental condition; For PHE adsorption study, BMPCs dosage was 0.05g/L, initial PHE concentration 0.6mg/L, solution volume 40mL, pH 6.4-6.8, and temperature 25℃. For phenol, BMPCs dosage was 0.25g/L, initial phenol concentration 10mg/L, solution volume 40mL, pH 6.4-6.8, and temperature 25℃. For 2,4,6-TCP, BMPCs dosage o.25g/L, initial 2,4,6-TCP concentration 50mg/L, solution volume 40mL, pH 6.4-6.8, and temperature 25℃. The original figures corresponding to figure B, E and I are in supplementary information (Figure S3).

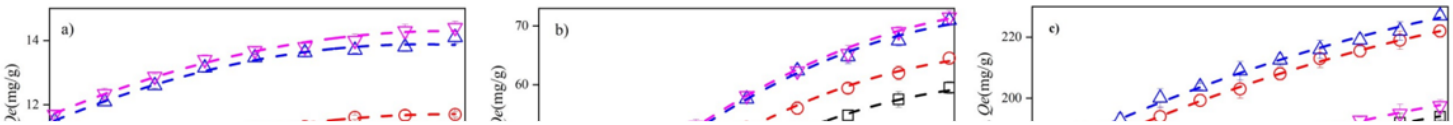

Figure 5

Adsorption equilibrium parameters for PHE, phenol and 2,4,6-TCP on BMPCs. Experimental conditions: For PHE adsorption study, BMPCs dosage 0.05g/L, initial PHE concentration 600-1000μg/L, pH 6.4-6.8, equilibrium time is three days, temperature 25°C. For phenol and 2,4,6-trichlorophenol, BMPCs dosage 0.25g/L, initial phenol concentration 10-50mg/L and initial 2 ,4,6-TCP concentration 50-100mg/L, pH 6.4-6.8 equilibrium time is one day, temperature 25°C. Isotherm data were fitted to Langmuir and Freundlich model. Error bars indicate standard deviation.

Figure 6

FTIR spectra of BMPCs before and after adsorption of PHE, phenol and 2,4,6-TCP.

Supplementary Files

This is a list of supplementary files associated with this preprint. Click to download.

- GraphicalAbstract.png
- Supplementaryinformation.docx